*applied sciences*

MDPI

*Article*

# A Stability Analysis on Mixed Convection Boundary Layer Flow along a Permeable Vertical Cylinder in a Porous Medium Filled with a Nanofluid and Thermal Radiation

**Shahirah Abu Bakar [1], Norihan Md Arifin [1,2,*], Fadzilah Md Ali [1,2], Norfifah Bachok [1,2], Roslinda Nazar [3] and Ioan Pop [4]**

1 Institute for Mathematical Research, Universiti Putra Malaysia, UPM Serdang, Selangor 43400, Malaysia; shirabubakar@yahoo.com.my (S.A.B.); fadzilahma@upm.edu.my (F.M.A.); norfifah@upm.edu.my (N.B.)
2 Department of Mathematics, Faculty of Science, Universiti Putra Malaysia, UPM Serdang, Selangor 43400, Malaysia
3 School of Mathematical Sciences, Faculty of Science and Technology, Universiti Kebangsaan Malaysia, UKM Bangi, Selangor 43600, Malaysia; rmn72my@yahoo.com
4 Department of Mathematics, Babes-Bolyai University, Cluj-Napoca R-400084, Romania; pop.ioan@yahoo.co.uk
* Correspondence: norihana@upm.edu.my; Tel.: +603-8946-7266

Received: 1 February 2018; Accepted: 25 February 2018; Published: 23 March 2018

**Abstract:** A study on mixed convection boundary layer flow with thermal radiation and nanofluid over a permeable vertical cylinder lodged in a porous medium is performed in this current research by considering groupings of a variety nanoparticles, consisting of copper (Cu), aluminium ($Al_2O_3$) and titanium ($TiO_2$). By using a method of similarity transformation, a governing set of ordinary differential equations has been reduced from the governing system of nonlinear partial differential equations, which are the values of selected parameters such as mixed convection parameter $\lambda$, nanoparticle volume fraction $\varphi$, radiation parameter $Rd$, suction parameter $S$, and curvature parameter $\xi$ are solved numerically. From the numerical results, we observed that the involving of certain parameters ranges lead to the two different branches of solutions. We then performed a stability analysis by a bvp4c function (boundary value problem with fourth-order accuracy) to determine the most stable solution between these dual branches and the respective solutions. The features have been discussed in detail.

**Keywords:** mixed convection; cylinder; nanofluid; porous medium; thermal radiation; stability analysis

## 1. Introduction

A better understanding of heat transfer and boundary layer flow through a permeable surface can benefit several important areas, especially in technology and engineering fields, in such applications as wire drawing, glass-fiber and paper production, and insulation design, to name a few. Further, an innovative technique to improve heat transfer known as nanofluid has been extensively used during these last decades because the traditional heat transfer fluids are known to behave poorly in terms of heat transfer. The nanofluid term was first introduced by Choi [1], and is defined as a fluid capable of suspending nanoscale particles in the base fluid. Basically, the nanoparticles are constructed from carbon, aluminium, copper, and generally come from chemically stable materials. The nanofluid concept has been introduced and improvised as a method of enhancing the heat transfer performance rates in liquids. Materials in the size of nanometers possess unique chemical and physical properties, since nanofluids make it possible for these materials to flow smoothly through microchannels without clogging because of their small size, as they behave similarly to liquid molecules [2]. This fact has attracted researchers to perform investigations on heat transfer characteristics through nanofluids. Several authors [3–6] have extensively studied and analyzed the effects of nanofluids on heat transfer.

In an area of fluid dynamics, the flow of potential around a circular cylinder is a solution to allow the flow of an incompressible and inviscid flow around a cylinder that is transverse to the flow itself. A boundary layer is created where the surface of a velocity is at zero value and transforms to the value of the free stream some distance away from the cylinder surface. When the boundary layer thickness is less than the radius of cylinder, then the flow is considered to be two-dimensional. To the contrary, the thickness of the boundary layer may be the same order of the cylinder radius in the case of a thin or slender cylinder. Therefore, instead of considering the flow as two-dimensional, it is more accurate that the flow be considered as an axisymmetric flow (see [7]). Due to this reason, the research of mixed convection through a cylinder has lead to an excellent collection of articles such as by [8–11].

At the same time, considerable progress on the understanding of radiative heat transfer in flow processes in industry and engineering fields is very important since it is one of the three fundamental modes of heat transfer. Thermal radiation can be explained as electromagnetic radiation generated by charged particles of thermal motion in matter. The effects of thermal radiation are of considerably interest in flow processing at a high temperature, because the radiation can significantly influence the participating fluids' heat transmit rate, as well as the temperature distribution in the flow of the boundary layer when temperatures are high. Considerable research in the area of thermal radiation have been proposed recently, and the concept of thermal radiation is still of significant interest, as it may provide better results to affect the kinematic flows and achieve a suitable control on the cooling rate in such a way as to ensure the solidification at a slower rate than other well-known methods. Here we study the steady, two-dimensional mixed convection boundary layer flow, with thermal radiation filled with a nanofluid along a permeable vertical cylinder lodged in a porous medium, where we apply the mathematical model as presented by Tiwari and Das [12], which is also extended by Rohni et al. [13]. Copper (Cu), aluminium ($Al_2O_3$) and titanium ($TiO_2$) are among the nanoparticles reviewed in this study, and by performing a similarity transformation method, a set of ordinary differential equations has been reduced from the governing partial differential equations system. The corresponding ordinary differential equations were solved numerically by the shooting technique method in Maple software (Maple 16, Maplesoft, Waterloo, ON, Canada, 2003). Further, a method named stability analysis is performed to determine the stability of the obtained dual solutions.

## 2. Mathematical Formulation

Consider a two-dimensional, steady mixed convection boundary layer flow embedded in a porous medium along a permeable vertical cylinder with radius $a$, which is filled with thermal radiation and a nanofluid, as illustrated in Figure 1.

By considering these assumptions alongside the boundary layer and Boussinesq approximations, the respective system of continuity, momentum and energy are:

$$\frac{\partial (ru)}{\partial x} + \frac{\partial (rv)}{\partial r} = 0, \tag{1}$$

$$\frac{\mu_{nf}}{\mu_f}\frac{\partial u}{\partial r} = \frac{gK\left[\varphi\rho_s\beta_s + (1-\varphi)\rho_f\beta_f\right]}{\mu_f}\frac{\partial T}{\partial r}, \tag{2}$$

$$u\frac{\partial T}{\partial x} + v\frac{\partial T}{\partial r} = \frac{\alpha_{nf}}{r}\frac{\partial}{\partial r}\left(r\frac{\partial T}{\partial r}\right) - \frac{1}{(\rho C_p)_{nf}}\left(\frac{\partial q_r}{\partial r}\right), \tag{3}$$

subjected to the boundary conditions as follows:

$$\begin{array}{c} v = v_w,\ T = T_\infty + T_0\frac{x}{a} \text{ on } r = a, \\ u \to U_0\frac{x}{a},\ T \to T_\infty \text{ as } r \to \infty. \end{array} \tag{4}$$

Here $r$ and $x$ are the cylindrical coordinates measured over the cylinder axes, $u$ and $v$ are the components of velocity over the $x$ and $r$-axes, $g$ is gravity acceleration, $T$ is temperature, $\varphi$ is nanoparticle volume fraction, $\rho$ is fluid density, $\beta$ is the coefficient of thermal expansion, $\alpha$ is thermal diffusivity, $\mu$ is viscosity, $q_r$ is the heat flux of radiative and the subscripts of $nf$, $f$ and $s$ correspond to the nanofluid, fluid and solid, respectively. Using Rosseland's approximation for radiation [14], we have $q_r = \frac{-4\sigma}{3k*}\frac{\partial T^4}{\partial r}$ where $k*$ is the coefficient of mean absorption and $\sigma$ is Stefan Boltzmann constant. The temperature differences are significantly small within the flow so that $T^4$ may be considered as a temperature linear function $T$ by using a Taylor series of truncated about the temperature of free stream $T_\infty$, and we get $T^4 \approx 4T_\infty^3 T - 3T_\infty^4$. Equation (3) now can be reduced to:

$$u\frac{\partial T}{\partial x} + v\frac{\partial T}{\partial r} = \frac{\alpha_{nf}}{r}\frac{\partial}{\partial r}\left(r\frac{\partial T}{\partial r}\right) + \frac{16\sigma T_\infty^3}{3k * (\rho C_p)_{nf}}\frac{\partial^2 T}{\partial r^2}. \tag{5}$$

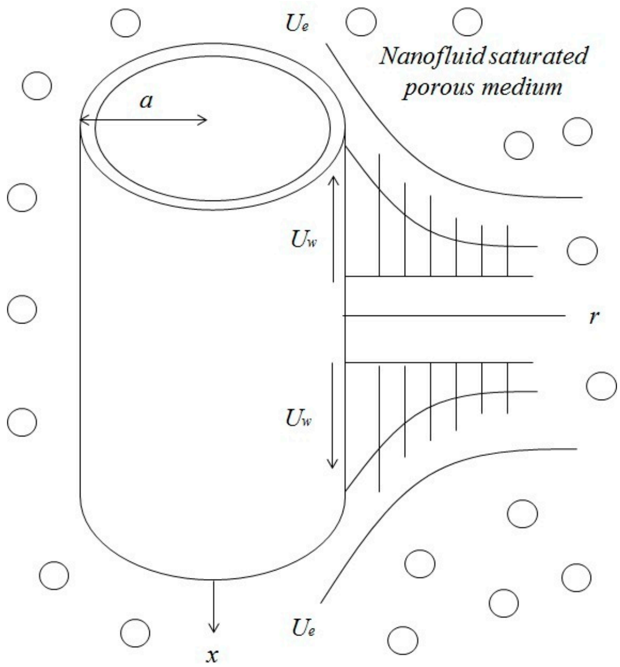


**Figure 1.** Physical model of the present problem.

The physical properties of nanofluids as stated in Equations (3) and (5) are given by [15]:

$$\begin{array}{c} \mu_{nf} = \frac{\mu_f}{(1-\varphi)^{2.5}},\ \alpha_{nf} = \frac{k_{nf}}{(\rho C_p)_{nf}},\ \rho_{nf} = (1-\varphi)\rho_f + \varphi\rho_s, \\ (\rho C_p)_{nf} = (1-\varphi)(\rho C_p)_f + \varphi(\rho C_p)_s,\ \frac{k_{nf}}{k_f} = \frac{(k_s+2k_f)-2\varphi(k_f-k_s)}{(k_s+2k_f)+\varphi(k_f-k_s)}, \end{array} \tag{6}$$

where $\rho C_p$ is heat capacitance. We now introduce the following similarity variables:

$$\psi = \sqrt{2U_0 a\alpha_f}\, x f(\eta),\ T = T_\infty + \frac{T_0 x}{a}\theta(\eta),\ \eta = \frac{r^2 - a^2}{2a\alpha_f}\sqrt{\frac{U_0\alpha_f}{2a}}. \tag{7}$$

Substituting Equation (7) into Equations (3) and (5), we can reduce the governing system as follows:

$$f'' + B\lambda\theta' = 0, \tag{8}$$

$$\left[A(1+2\xi\eta) + \frac{8}{3}\xi Rd\right]\theta'' + \left(2A\xi + \frac{8}{3}\xi Rd\right)\theta' + 2f\theta' - 2f'\theta = 0, \tag{9}$$

subjected to the boundary conditions:

$$\begin{array}{c} f(0) = S, \theta(0) = 1, \\ f'(\eta) \to 1, \theta(\eta) \to 0 \text{ as } \eta \to \infty, \end{array} \tag{10}$$

where $\lambda$ is the parameter of mixed convection, $\xi$ is curvature parameter, $Rd$ is radiation parameter and $S$ is suction parameter. These parameters, together with the constants $A$ and $B$ are given by as follows:

$$\begin{array}{c} \lambda = \frac{Ra_x}{Pe_x}, \xi = \left(\frac{2\alpha_f}{U_0 a}\right)^{1/2}, Rd = \frac{4\sigma T_\infty^3}{k*U_0\alpha_f}, S = \frac{-v_w}{U_0\alpha_f}, \\ A = \frac{k_{nf}/k_f}{(1-\varphi)+\varphi(\rho C_p)_s/(\rho C_p)_f}, B = (1-\varphi)^{2.5}\left[(1-\varphi) + (\rho\beta)_s/(\rho\beta)_f\right]. \end{array} \tag{11}$$

It is worth to mention that $\lambda < 0$ corresponds to opposing flow or cooled flow, $\lambda > 0$ corresponds to an assisting flow or heated plate, and while $\lambda = 0$ is flow of forced convection. Because of the porous medium characteristics, we can combined Equations (8) and (9) to give a single equation. However, we need to integrate Equation (8) first and applying the boundary conditions (10) to give:

$$f' - B\lambda\theta - 1 = 0. \tag{12}$$

By substituting Equation (12) into Equation (9), we obtained:

$$\left[A(1+2\xi\eta) + \frac{8}{3}\xi Rd\right]f''' + \left(2A\xi + \frac{8}{3}\xi Rd\right)f'' + 2ff'' - 2\left(f'\right)^2 + 2f' = 0, \tag{13}$$

alongside the new simplified boundary conditions:

$$\begin{array}{c} f(0) = S, f'(0) = B\lambda + 1, \\ f'(\eta) \to 1 \text{ as } \eta \to \infty. \end{array} \tag{14}$$

The practical interest of physical quantity is the skin friction coefficient $C_f$, in terms of the shear stress of dimensional wall $f''(0)$, which is defined as:

$$C_f = \frac{\tau_w}{\rho_f u_e^2}, \tag{15}$$

where $\tau_w$ is skin friction and given by:

$$\tau_w = \mu_{nf}\left(\frac{\partial u}{\partial r}\right)_{r=a}. \tag{16}$$

Substituting the dimensionless variables in Equation (7) into Equations (15) and (16), we have:

$$(2Pe_x)^{1/2}C_f = \frac{1}{(1-\varphi)^{2.5}}f''(0), \tag{17}$$

where $Pe_x = u_e(x)x/\alpha_f$ is local the Péclet number and $\Pr = \nu_f/\alpha_f$ is the local Prandtl number for porous medium.

## 3. Stability Analysis

In this respect, we consider the unsteady state of our governing model in order to perform an analysis of stability on the present problem. While Equation (1) remains the same, Equations (2) and (3) replaced by as follows:

$$\frac{\partial u}{\partial t}+\frac{\mu_{nf}}{\mu_f}\frac{\partial u}{\partial r}=\frac{gK\left[\varphi\rho_s\beta_s+(1-\varphi)\rho_f\beta_f\right]}{\mu_f}\frac{\partial T}{\partial r}, \tag{18}$$

$$\frac{\partial T}{\partial t}+u\frac{\partial T}{\partial x}+v\frac{\partial T}{\partial r}=\frac{\alpha_{nf}}{r}\frac{\partial}{\partial r}\left(r\frac{\partial T}{\partial r}\right)-\frac{1}{(\rho C_p)_{nf}}\left(\frac{\partial q_r}{\partial r}\right), \tag{19}$$

where $t$ is time. The new boundary conditions are now replaced by:

$$\begin{array}{c} t<0:\ u=v=0, T=T_\infty \text{ for any } x, r, \\ t\geq 0:\ v=v_w, T=T_\infty+T_0\frac{x}{a} \text{ at } r=0, \\ u\to U_0\frac{x}{a}, T\to T_\infty \text{ as } r\to\infty. \end{array} \tag{20}$$

A new dimensionless variable $\tau$ is now introduced, where $\tau$ is uniform with the problem of which solutions will be associates with an initial value problem and physically realizable. With the introduction of new dimensionless variable $\tau$ and Equation (7), we now have:

$$\psi=\sqrt{2U_0 a\alpha_f}\,xf(\eta), T=T_\infty+\frac{T_0 x}{a}\theta(\eta), \eta=\frac{r^2-a^2}{2a\alpha_f}\sqrt{\frac{U_0\alpha_f}{2a}}, \tau=at. \tag{21}$$

We substitute Equation (21) into Equations (18) and (19), and we get:

$$\frac{\partial^2 f}{\partial\eta^2}+B\lambda\frac{\partial\theta}{\partial\eta}+\frac{\partial^2 f}{\partial\eta\partial\tau}=0, \tag{22}$$

$$\left[A(1+2\xi\eta)+\frac{8}{3}\xi Rd\right]\frac{\partial^2\theta}{\partial\eta^2}+\left(2A\xi+\frac{8}{3}\xi Rd\right)\frac{\partial\theta}{\partial\eta}+2f\frac{\partial\theta}{\partial\eta}-2\frac{\partial f}{\partial\eta}\theta-2\frac{\partial\theta}{\partial\tau}=0. \tag{23}$$

It is worth mentioning that Equations (22) and (23) can be combined together because of the characteristic of porous medium to give a single equation as follows:

$$\begin{array}{c}\left[A(1+2\xi\eta)+\frac{8}{3}\xi Rd\right]\left(\frac{\partial^3 f}{\partial\eta^3}+\frac{\partial^3 f}{\partial\eta^2\partial\tau}\right)+\left(2A\xi+\frac{8}{3}\xi Rd\right)\frac{\partial^2 f}{\partial\eta^2}+\left(2A\xi+\frac{8}{3}\xi Rd-2+2f\right)\frac{\partial^2 f}{\partial\eta\partial\tau}- \\ 2\left(\frac{\partial f}{\partial\eta}\right)^2+2\frac{\partial f}{\partial\eta}+2f\frac{\partial^2 f}{\partial\eta^2}-2\frac{\partial\theta}{B\lambda\partial\tau}=0.\end{array} \tag{24}$$

The boundary conditions in Equation (20) now reduced to:

$$\begin{array}{c} f(0)=S, \frac{\partial f}{\partial\eta}(0)=B\lambda+1, \\ \frac{\partial f}{\partial\eta}(\eta)\to 1 \text{ as } \eta\to\infty. \end{array} \tag{25}$$

We test the solution stability of $f(\eta)=f_0(\eta)$ and $\theta(\eta)=\theta_0(\eta)$ to satisfy the boundary value problems as in Equation (14) by embraced the analysis proposed by Merkin [14] and Weidman et al. [15]:

$$f(\eta,\tau)=f_0(\eta)+e^{-\gamma\tau}F(\eta,\tau),\ \theta(\eta,\tau)=\theta_0(\eta)+e^{-\gamma\tau}G(\eta,\tau), \tag{26}$$

where $\gamma$ is the unknown eigenvalue or also can be described as the rate of growth or decay of disturbances. The eigenvalue solutions give a set of infinite eigenvalues $\gamma_1<\gamma_2<\gamma_3<\ldots$, and later, the initial decay of disturbances will appear if the smallest eigenvalue is a positive number, and by then we can deduce that the solution is stable and significantly realizable. If the smallest eigenvalue shows a negative number, the flow is said to be unstable by the meaning if there is an initial disturbances growth.

We substitute Equation (26) into Equation (24) to give a final equation:

$$\begin{aligned}&\left[A(1+2\xi\eta)+\tfrac{8}{3}\xi Rd\right]F_0''' + \left(2A\xi+\tfrac{8}{3}\xi Rd - A\gamma - 2A\gamma\xi\eta - \tfrac{8}{3}\gamma\xi Rd\right)F_0'' + \\ &\left(2-2A\gamma\xi-\tfrac{8}{3}\gamma Rd + 2\gamma - 2\gamma f_0 - 4f_0\right)F_0' + 2\gamma f_0 F_0'' + 2f_0'' F_0 + \tfrac{2\gamma G_0'}{B\lambda} = 0,\end{aligned} \tag{27}$$

subjected to the boundary conditions:

$$\begin{aligned}&F_0(0)=0, F_0'(0)=0,\\ &F'(\eta)\to 1 \text{ as } \eta\to\infty.\end{aligned} \tag{28}$$

The stability of dual solutions is determined by the smallest number of eigenvalue $\gamma$. The range of possible eigenvalues can be evaluated by relaxing the $F_0(\eta)$ on our initial boundary condition, see [16]. Thus, we choose a fixed value of $\gamma$ so that the condition of $F_0'(\eta)=0$ as $\eta\to\infty$ can be relaxed and the equations with the new boundary condition of $F_0'(\eta)=1$ as $\eta\to\infty$ can be solved numerically.

## 4. Results

A shooting technique method is performed in this section to obtain the numerical solutions for different values of involving parameters in our governing system of reduced ordinary differential equations in Equation (13), subjected to the boundary conditions (14). The respective results are given to carry out the influences of several kind of parameters on the parametric study, such as mixed convection parameter $\lambda$, radiation parameter $Rd$, suction parameter $S$, curvature parameter $\xi$, as well as nanoparticle volume fraction $\varphi$, on three nanoparticles types namely Cu (copper), $Al_2O_3$ (aluminium) and $TiO_2$ (titanium). It is worth mentioning that Table 1 lists the physical properties of base fluid and selected types of nanoparticle, while Table 2 shows the values of constants $A$ and $B$ as defined in Equations (8) and (9) by using the thermophysical properties of water and Cu-nanoparticles.

**Table 1.** Physical properties of selected nanoparticles and base fluid.

| Physical Properties | Fluid | Copper | Aluminium | Titanium |
|---|---|---|---|---|
| $C_p$ (K/kg K) | 4179 | 385 | 765 | 686.2 |
| $\rho$ (kg/m$^3$) | 997.1 | 8933 | 3970 | 4250 |
| $k$ (W/m K) | 0.613 | 400 | 40 | 8.9538 |
| $\beta\times 10^{-5}$ (1/K) | 21 | 1.67 | 0.85 | 0.9 |

**Table 2.** Values of constants $A$ and $B$ as defined in Equations (8) and (9) by using the physical properties of water and Cu-nanoparticles.

| $\varphi$ | A | B |
|---|---|---|
| 0.05 | 1.1673 | 0.8670 |
| 0.1 | 1.3553 | 0.7463 |
| 0.2 | 1.8089 | 0.5395 |

In this present study, the reduced skin friction coefficient values, $(2Pe_x)^{1/2}C_f$, for selected numbers of nanoparticle volume fraction parameter $\varphi$, against $\lambda$ when $Rd=S=0.1$ and $\xi=0.5$ for Cu-water nanoparticles are shown in Figure 2. The analysis shows that there are dual solutions obtained for certain range of $\lambda$ because of the uniqueness and existence of dual solutions depend on the mixed convection parameter $\lambda$. These regions of unique solutions are known as first solution (upper branch) and second solution (lower branch). The terms of upper and lower branches correspond to the bifurcation presences in the curves when $\lambda$ is in critical value. From Figure 2, we can see that the solution is unique for $\varphi = 0.05$ where the range of $\lambda$ is $-1.93591 \leq \lambda < 0$, followed by $\varphi = 0.1$ where the range of $\lambda$ is $-2.25488 \leq \lambda < 0$ and $\varphi = 0.2$ with the range of $\lambda$ is $-3.14057 \leq \lambda < 0$.

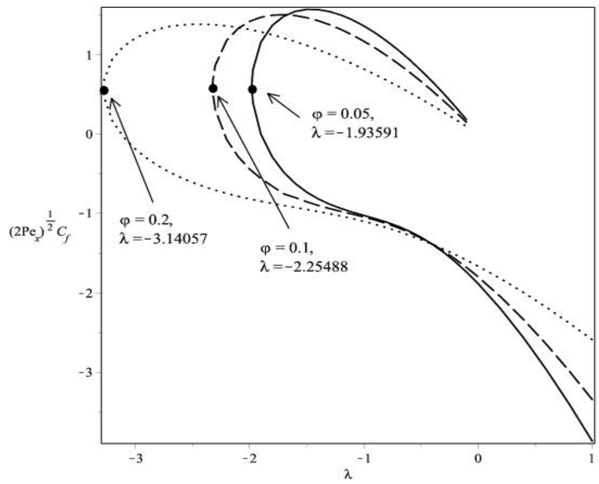


**Figure 2.** Skin friction coefficient $(2Pe_x)^{1/2}C_f$, for various values of $\varphi$ against $\lambda$ when $Rd = S = 0.1$ and $\xi = 0.5$ for Cu-nanoparticles.

Plots of the reduced skin friction coefficient $(2Pe_x)^{1/2}C_f$, for selected values of radiation parameter $Rd$, against $\lambda$ when other parameters are constant for Cu-nanoparticles are depicted in Figure 3. Meanwhile, Figure 4 illustrates the plots of skin friction coefficient $(2Pe_x)^{1/2}C_f$, for selected values of suction parameter $S$, in the case of Cu-water. Similar with those $(2Pe_x)^{1/2}C_f$ in Figure 2, dual solutions are obtained for certain range of $\lambda$ when $Rd$ and $S$ are increasing. From these two figures, we noticed that the range of $\lambda$ is increasing when the parameters $Rd$ and $S$ increase.

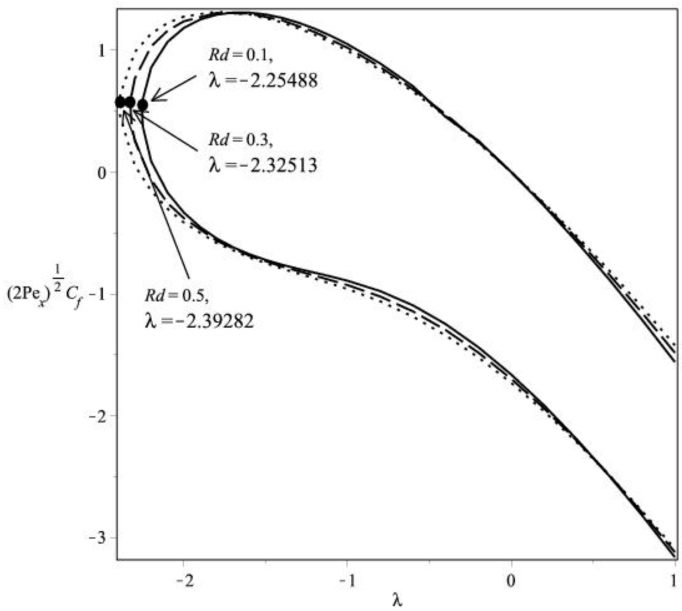


**Figure 3.** Skin friction coefficient $(2Pe_x)^{1/2}C_f$, for various values of $Rd$ against $\lambda$ when $\varphi = S = 0.1$ and $\xi = 0.5$ for Cu-nanoparticles.

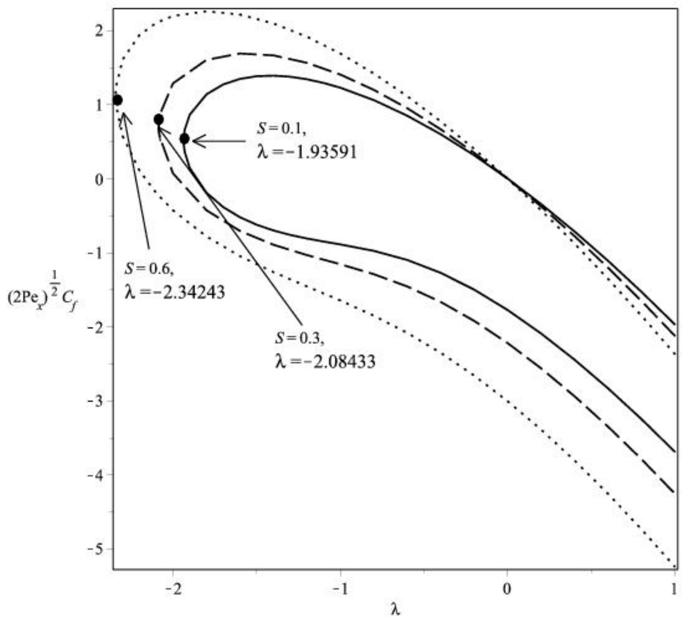


**Figure 4.** Skin friction coefficient $(2Pe_x)^{1/2}C_f$, for selected values of $S$ against $\lambda$ when $\varphi = 0.05$, $Rd = 0.1$ and $\xi = 0.5$ for Cu-nanoparticles.

We now consider velocity profiles $f'(\eta)$, as illustrated in Figure 5, for selected values of mixed convection parameter $\lambda$, when $\varphi = Rd = S = 0.1$ and $\xi = 0.5$ for three types of nanoparticles and it is clearly seen that both solutions increase when $\lambda$ increases. The reason behind these increasing/decreasing patterns is because the buoyancy force behaves like a pressure gradient which causes the fluid to accelerate or decelerate within the boundary layer. In addition, Figure 6 shows the various values of nanoparticle volume fraction parameter $\varphi$ on velocity profiles $f'(\eta)$, when $\lambda = -1.6$, $Rd = S = 0.1$ and $\xi = 0.5$ for Cu, $Al_2O_3$ and $TiO_2$ nanoparticles. For these three types of nanoparticles, both the first and second solutions decrease when values of $\varphi$ increasing.

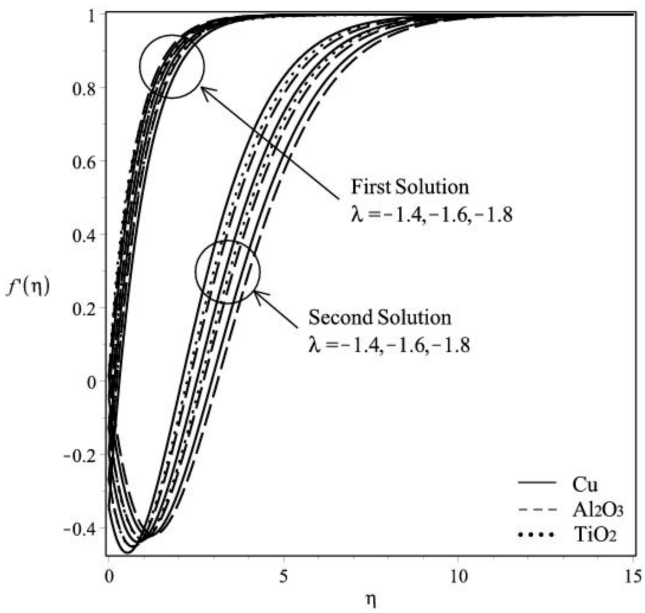


**Figure 5.** Various values of $\lambda$ on velocity profiles $f'(\eta)$, when $\varphi = Rd = S = 0.1$ and $\xi = 0.5$ for three types of nanoparticles.

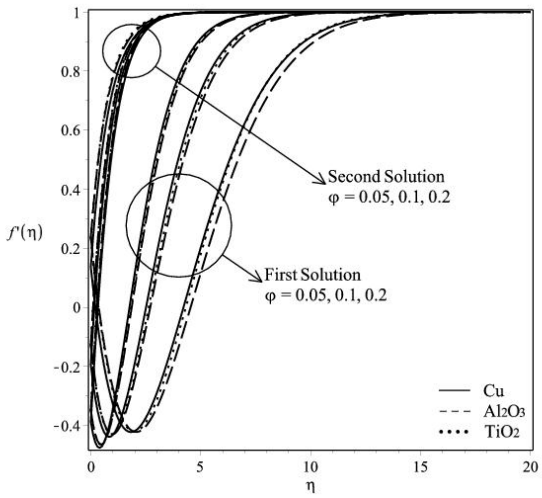


**Figure 6.** Various values of $\varphi$ on velocity profiles $f'(\eta)$, when $\lambda = -1.6$, $Rd = S = 0.1$ and $\xi = 0.5$ for three types of nanoparticles.

In order to explore the thermal radiation parameter $Rd$, influences on $f'(\eta)$ for all three types of nanoparticles, we set a constant value of $\varphi = S = 0.1$, $\lambda = -1.5$ and $\xi = 1.0$ as depicted in Figure 7, while Figure 8 shows the numerous values of suction parameter $S$ on velocity profiles $f'(\eta)$, for copper, aluminium and titanium nanoparticles, and taking this account into are $\varphi = 0.05$, $Rd = 0.1$, $\lambda = -1.6$ and $\xi = 0.5$. From Figure 7, we noticed that both solutions are decreasing when parameter $Rd$ increases. It is worth to know that the radiation effect is to escalate the rate of heat transfer, thus radiation should be at its minimum value in order to ease the cooling process, or else the higher number of radiation might taking a slow process of heat transfer. On the other hand, we confirmed that the first solution is increasing, while the second solution is conversely decreasing when parameter $S$ increasing as in Figure 8. This is due to the fact that the flow in the first solution of boundary layer is taken up by suction, and thus sparks an enhancing energy on the same matter. Not stopping here, we consider the influences of curvature parameter $\xi$, on velocity profiles $f'(\eta)$, for three kinds of nanoparticles when $\lambda = -1.6$ and $\varphi = Rd = S = 0.1$ as illustrated in Figure 9. From this result, we can clearly observed that the thickness of the boundary layer is increasing in both the first and second solutions when the value of $\xi$ increasing.

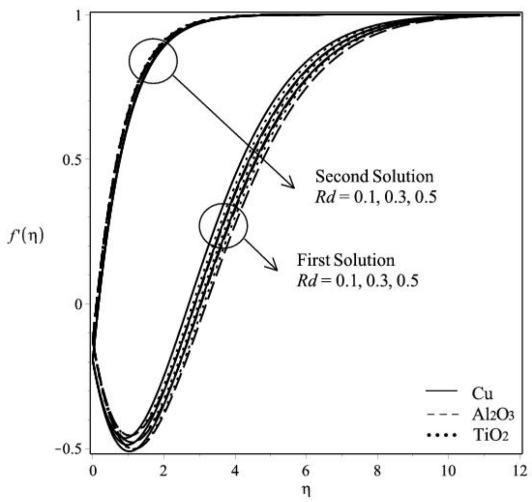


**Figure 7.** Various values of $Rd$ on velocity profiles $f'(\eta)$, when $\varphi = S = 0.1$, $\lambda = -1.5$ and $\xi = 1.0$ for three types of nanoparticles.

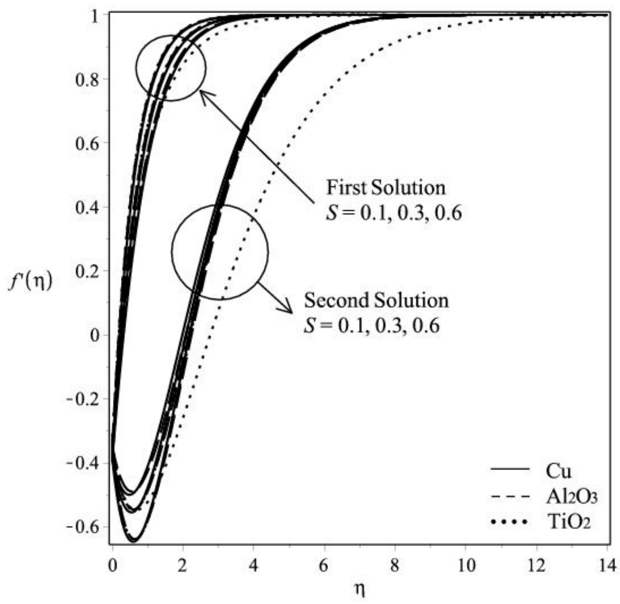


**Figure 8.** Various values of $S$ on velocity profiles $f'(\eta)$, when $\varphi = 0.05$, $Rd = 0.1$, $\lambda = -1.6$ and $\xi = 0.5$ for three types of nanoparticles.

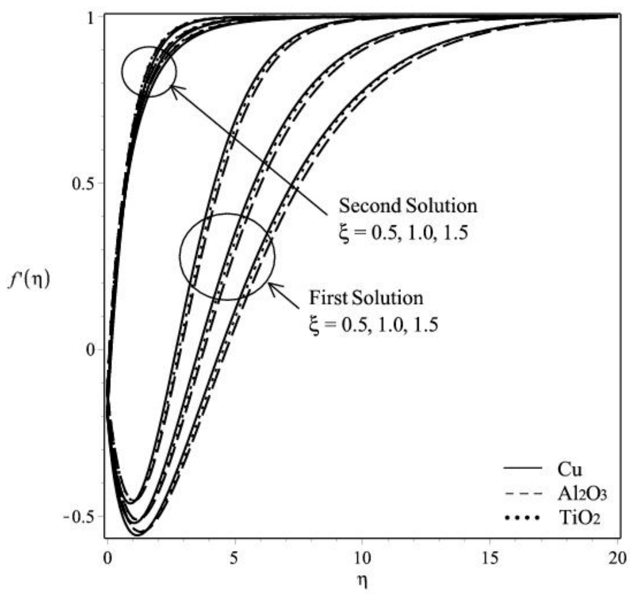


**Figure 9.** Various values of $\xi$ on velocity profiles $f'(\eta)$, when $\varphi = Rd = S = 0.1$ and $\lambda = -1.6$ for three types of nanoparticles.

Due to the existence of dual solutions in a selected range of parameters, as shown in our respective numerical results, an analysis of stability is performed in order to determine the most stable solution between these two solutions by finding the smallest eigen value $\gamma$. The eigenvalue solutions as in Equation (27), subjected to the boundary conditions (28), were numerically programmed in MATLAB software (Matlab R2017a, MathWorks, Natick, MA, USA, 1984) by using a bvp4c function. The selected values of $\lambda$ together with the smallest eigenvalue $\gamma$ for three types of nanoparticles are properly listed in Table 3, when other parameters such as $\varphi = Rd = S = 0.1$ and $\xi = 0.5$. Meanwhile, Table 4 listed the smallest eigenvalue $\gamma$ for various values of radiation parameter $Rd$, when $\varphi = S = 0.1$, $\lambda = -1.6$ and $\xi = 0.5$ for Cu, $Al_2O_3$ and $TiO_2$ nanoparticles. From these two tables, it is observed that the first solutions (upper branches) show positive values, while second solutions (lower branches) show negative values. Right at this moment, we can finally conclude that the first solution is stable and significantly realizable, and second solution is said to be unstable and not physically realizable.

**Table 3.** List of several values of $\lambda$ and the smallest eigenvalue $\gamma$ when $\varphi = Rd = S = 0.1$ and $\xi = 0.5$ for three types of nanoparticles.

| $\lambda$ | Copper | | Aluminium | | Titanium | |
|---|---|---|---|---|---|---|
| | First Solution | Second Solution | First Solution | Second Solution | First Solution | Second Solution |
| −1.3 | 0.59663 | −0.64225 | 0.27145 | −0.36161 | 0.22169 | −0.32238 |
| −1.4 | 0.69092 | −0.74210 | 0.32588 | −0.42126 | 0.24201 | −0.37918 |
| −1.5 | 0.78522 | −0.84195 | 0.38032 | −0.48091 | 0.26233 | −0.43597 |
| −1.6 | 0.87951 | −0.94180 | 0.43474 | −0.54055 | 0.28265 | −0.49276 |

**Table 4.** List of several values of $Rd$ and the smallest eigenvalue $\gamma$ when $\varphi = S = 0.1$, $\gamma = -1.6$ and $\xi = 0.5$ for three types of nanoparticles.

| Rd | Copper | | Aluminium | | Titanium | |
|---|---|---|---|---|---|---|
| | First Solution | Second Solution | First Solution | Second Solution | First Solution | Second Solution |
| 0.2 | 0.78526 | −0.84201 | 0.38032 | −0.48132 | 0.26269 | −0.43730 |
| 0.4 | 0.78535 | −0.84211 | 0.38035 | −0.48214 | 0.26339 | −0.44001 |
| 0.6 | 0.78544 | −0.84221 | 0.38038 | −0.48297 | 0.26406 | −0.44227 |
| 0.8 | 0.78553 | −0.84232 | 0.38041 | −0.48381 | 0.26471 | −0.44560 |

## 5. Conclusions

The study of a stability analysis on mixed convection boundary layer flow filled with nanofluid and thermal radiation over a permeable vertical cylinder lodged in a porous medium has been numerically analyzed and discussed in detail in this paper. It was found that the involving parameters—specifically the mixed convection parameter $\lambda$, radiation parameter $Rd$, suction parameter $S$, nanoparticle volume fraction $\varphi$ and curvature parameter $\xi$—significantly affected the flow field. We can observe that for the three kinds of nanoparticles, $Al_2O_3$ and $TiO_2$ are shown to separate the boundary layer thickness faster—which do not have much difference, and is followed by Cu. We then performed an analysis of stability on the respective model since there exists dual solutions obtained by a selected range of parameters. The main purpose of stability analysis is to analyze the most stable solution from the two solutions obtained from our numerical results. It has been identified that the first solution initiated decaying disturbances, while the second solution initiated growing disturbances. From this observation, we can make a final conclusion that the first solution is stable and physically realizable, while the second solution is not.

**Acknowledgments:** The authors gratefully acknowledge the financial support received in the form of a FRGS research grant from the Ministry of Higher Education, Malaysia.

**Author Contributions:** Norihan Md Arifin, Fadzilah Md Ali, Norfifah Bachok and Roslinda Nazar conceived and designed the experiments; Shahirah Abu Bakar performed the experiments, analyzed the data and wrote the paper; Norihan Md Arifin and Ioan Pop re-checked the experiments to make sure it is correct.

**Conflicts of Interest:** The authors declare no conflicts of interest.

## Nomenclatures

| | |
|---|---|
| $a$ | Radius |
| $\alpha$ | Thermal diffusivity |
| $\beta$ | Fluid thermal expansion coefficient |
| $C_f$ | Skin friction coefficient |

| | |
|---|---|
| $\eta$ | Similarity variable |
| $g$ | Gravity acceleration |
| $\gamma$ | Unknown eigenvalue |
| $k$ | Fluid thermal conductivity |
| $k^*$ | Mean absorption coefficient |
| $K$ | Porous media permeability |
| $\lambda$ | Mixed convection parameter |
| $\mu$ | Fluid viscosity |
| $Pe_x$ | Peclet number |
| $\psi$ | Stream function |
| $q_r$ | Radiative heat flux |
| $Rd$ | Radiation parameter |
| $\rho$ | Fluid density |
| $\rho C_p$ | Heat capacitance |
| $S$ | Suction parameter |
| $\sigma$ | Stefan–Boltzmann constant |
| $t$ | Time |
| $T$ | Temperature |
| $T_0$ | Constant for heated/cooled cylinder |
| $T_\infty$ | Free stream temperature |
| $T^4$ | Linear function of temperature |
| $\tau$ | Dimensionless variable for time |
| $\tau_w$ | Shear stress at the plate surface |
| $\theta$ | Nondimensionless temperature |
| $U_0$ | Constant for free stream velocity |
| $u, v$ | Velocity components along the $x$ and $r$ axes |
| $\varphi$ | Nanoparticle volume fraction parameter |
| $\xi$ | Curvature parameter |
| $x, r$ | Cylindrical coordinates measured along the cylindrical axes |

## References


1. Choi, S.U.S. Enhancing thermal conductivity of fluids with nanoparticles. *Int. Mech. Eng. Congr. Expos.* **1995**, *231*, 99–106.
2. Khanafer, K.; Vafai, K.; Lighstone, M. Buoyancy-driven heat transfer enhancement in a two-dimensional enclosure utilizing nanofluids. *Int. J. Heat Mass Transf.* **2003**, *46*, 3639–3653. [CrossRef]
3. Wang, X.; Xu, X.; Choi, S.U.S. Thermal conductivity of nanoparticles fluid mixture. *J. Thermophys. Heat Transf.* **1999**, *13*, 474–480. [CrossRef]
4. Ahmad, S.; Pop, I. Mixed convection boundary layer flow from a vertical flat plate embedded in a porous medium filled with nanofluids. *Int. J. Commun. Heat Mass Transf.* **2010**, *37*, 987–991. [CrossRef]
5. Bachok, N.; Ishak, A.; Pop, I. Stagnation-point flow over a stretching/shrinking sheet in a nanofluid. *Nano Res. Lett.* **2011**, *6*, 1–10. [CrossRef] [PubMed]
6. Arifin, N.M.; Nazar, R.; Pop, I. Free- and mixed convection boundary layer flow past a horizontal surface embedded in a porous medium filled with a nanofluid. *J. Thermophys. Heat Transf.* **2012**, *26*, 375–382. [CrossRef]
7. Datta, P.; Anilkumar, D.; Roy, S.; Mahanti, N. Effect of non-uniform slot injection (suction) on forced flow over a slender cylinder. *Int. J. Heat Mass Transf.* **2006**, *49*, 2366–2371. [CrossRef]
8. Costa, V.; Raimundo, A. Steady mixed convection in a differentially heated square enclosure with an active rotating circular cylinder. *Int. J. Heat Mass Transf.* **2010**, *53*, 1208–1219. [CrossRef]
9. Nazar, R.; Tham, I.; Pop, I.; Ingham, D. Mixed convection boundary layer flow from a horizontal circular cylinder embedded in a porous medium filled with a nanofluid. *Transp. Porous Media* **2011**, *86*, 517–536. [CrossRef]
10. Khanafer, K.; Aithal, S. Laminar mixed convection flow and heat transfer characteristics in a lid drive cavity with a circular cylinder. *Int. J. Heat Mass Transf.* **2013**, *66*, 200–209. [CrossRef]

11. Hayat, T.; Waqas, M.; Shehzad, S.A.; Alsaedi, A. Mixed convection flow of viscoelastic nanofluid by a cylinder with variable thermal conductivity and heat source/sink. *Int. J. Numer. Methods Heat Fluid Flow* **2016**, *26*, 214–234. [CrossRef]
12. Tiwari, R.K.; Das, M.K. Heat transfer augmentation in a two-sided lid-driven differentially heated square cavity utilizing nanofluids. *Int. J. Heat Mass Transf.* **2007**, *50*, 2002–2018. [CrossRef]
13. Rohni, A.M.; Ahmad, S.; Merkin, J.H.; Pop, I. Mixed convection boundary layer flow along a vertical cylinder embedded in a porous medium filled by a nanofluid. *Trans. Porous Media* **2013**, *96*, 237–253. [CrossRef]
14. Merkin, J. On dual solutions occurring in mixed convection porous medium. *J. Eng. Math.* **1986**, *20*, 171–179. [CrossRef]
15. Weidman, P.D.; Kubitschek, D.; Davis, A. The effect of transpiration on self-similar boundary layer flow over moving surfaces. *Int. J. Eng. Sci.* **2006**, *44*, 730–737. [CrossRef]
16. Harris, S.D.; Ingham, D.B.; Pop, I. Mixed convection boundary layer flow near the stagnation point on a vertical surface in a porous medium: Brinkman model with slip. *Trans. Porous Media* **2009**, *77*, 267–285. [CrossRef]